Cure Shrinkage Characterization of a Thermosetting Resin with Three-Dimensional Digital Image Correlation (3D-DIC)

KALIMA BUKENYA, ALESSANDRO SABATO and MARIANNA MAIARÙ

ABSTRACT

This work presents the application of three-dimensional digital image correlation (3D-DIC) to capture pre- and post-gelation volumetric chemical shrinkage of EPON 862 thermosetting resin paired with hardener triethylenetetramine (TETA) and cured at room temperature. The manufacturer-recommended 100:14 resin-hardener mixing ratio is used for DIC experimentation. A stress-free boundary condition is employed with a thin Teflon sheet placed between the resin mixture and the specimen container. For the first time, a spray-painted speckle pattern is applied directly to the resin to record full-field strain measurements during curing. This speckle pattern is employed immediately after the resin mixture is poured on the Teflon-covered specimen container for the pre-gelation case, and after gelation has been visibly observed for the post-gelation case. Strain capture with 3D-DIC is initiated directly after speckle pattern application with stereo-images captured every 30 seconds for one hour and then every 60 seconds for two hours. Differential scanning calorimetry (DSC) is used to determine resin cure kinetics to correlate chemical shrinkage with degree of cure. The presented technique provides an innovative methodology to characterize the chemical shrinkage of thermosets during curing.

INTRODUCTION

From the creation of plywood by the ancient Mesopotamians in the 4th millennium B.C. to the invention of the carbon fiber 3D printer by MarkForged in the 21st century, composites have remained a symbol of technological innovation and a catalyst for the advancement of human civilization. As present-day society looks toward the future of advanced materials, polymer matrix composites (PMCs) have become increasingly important across various engineering fields due to their high specific properties and low production costs [1–14]. Thermosetting resins are a class of polymers that undergo polymerization where monomers combine to form

University of Massachusetts Lowell, 1 University Avenue, Lowell, MA 01854, U.S.A.

cross-linked polymer chains during curing. Volumetric chemical shrinkage is a byproduct of polymerization and a driving factor for residual stress development and subsequent under-performance in thermoset composites [15–19]. Multiscale process modeling is an emerging field in materials engineering that leverages numerical modeling methods with characterized neat resin properties to predict cure-induced residual stresses and mechanical response [3, 19]. Chemical shrinkage must therefore be accurately characterized to fully understand the influence of the cure cycle and optimize composite performance [3, 20–23].

A crucial component of chemical shrinkage characterization lies in the capture of the phase change as the material solidifies from its liquid state. Several experimental practices have been developed to measure the volumetric shrinkage of thermoset resins. These methods are commonly designated as volume dilatometric and non-volume dilatometric. Volume dilatometers directly measure volumetric changes to derive chemical shrinkage and are classified as plunger-type, capillary type, and gravimetric [24–26]. Non-volume dilatometric procedures obtain shrinkage measurements through contacting or non-contacting transducers [27–29]. Examples of shrinkage measurement strategies under this category include density variation [30, 31], fibre Bragg grating (FBG) [32–34], and rheology [3, 35]. A detailed evaluation of volume and non-volume dilatometric techniques is found in Nawab et al [36]. The choice between a volume and a non-volume dilatometric technique is dependent on the processing constraints of the material, and many methods require an additional procedure such as differential scanning calorimetry (DSC) to characterize degree of cure.

Digital image correlation (DIC) has emerged as a promising optical method of measuring volumetric chemical shrinkage [37–39]. Recent studies have used two-dimenational (2D-) and three-dimensional DIC (3D-DIC) to record post-gelation shrinkage behaviors [40] and in-situ shrinkage evolution during autoclave processing [41]. Volumetric changes were tracked with a printed speckle pattern on a thin film adhered to the resin. Singer et al. used 3D-DIC and a fine SiC powder applied to the liquid resin surface to characterize shrinkage of polymer adhesive anchor systems with 3D-DIC [42]. Bukenya et al. employed 3D-DIC to characterize chemical shrinkage in a thermoset resin before and after gelation, and observed excellent agreement with validation data from rheology [43].

The proposed work applies 3D-DIC with stereovision cameras to investigate preand post-gelation chemical shrinkage stress-free strain fields as a function of degree of cure for thermosetting resin EPON 862 and curing agent TETA. DSC is used to predict degree of cure evolution.

This manuscript is outlined as follows. The upcoming section provides the theory, materials, and experimental methods employed during this study. Results are then shown and discussed in the succeeding section. Main conclusions are drawn in the final section.

METHODOLOGY

The resin chosen for this study includes the low-viscosity thermosetting resin produced by Hexion Inc. and commercially sold as EPONTM Resin 862. It was coupled with EPIKURETM Curing Agent 3234, also known as triethylenetetramine (TETA), to allow for a room-temperature cure. The material system presented in this work (henceforth referred to as EPON 862/TETA) was mixed with a stoichiometric ratio of 100:14 as recommended in the manufacturer safety data sheet. A schematic of the molecular structures for EPON 862 and TETA are shown below in Figure 1.

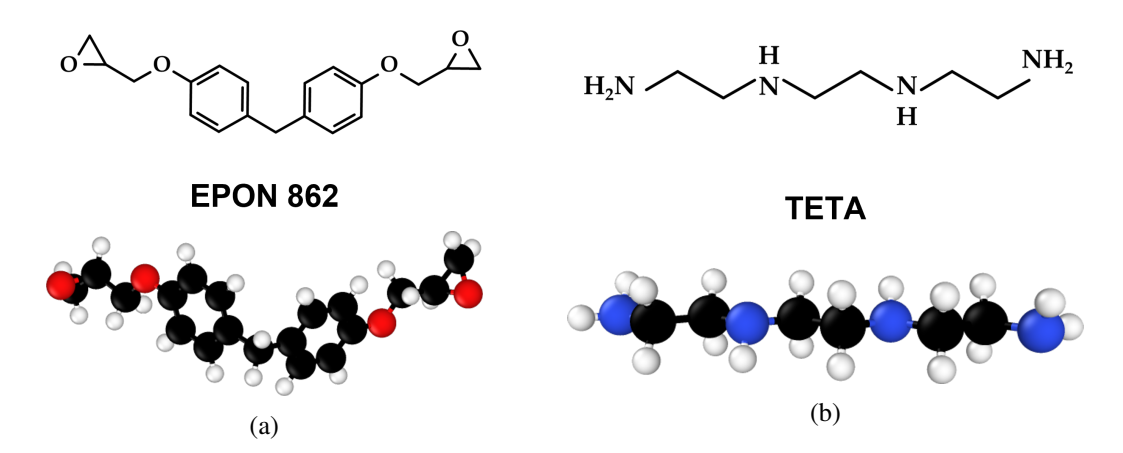


Figure 1. Molecular structure of (a) EPON resin 862 and (b) curing agent TETA.

Cure Kinetics

Thermoset resins such as EPON 862 undergo phase changes that result in chemical shrinkage. The degree of cure ϕ is given as:

$$\phi = \frac{H(t)}{H_T} \tag{1}$$

where H(t) is the partial heat generation term with respect to time t and H_T is the total heat of reaction. The cure rate $\frac{d\phi}{dt}$ is expressed as:

$$\frac{d\phi}{dt} = f(T, \phi) \tag{2}$$

For this study, a phenomenological semi-empirical cure kinetics model developed by Kamal [44] was chosen to represent the cure evolution.

$$f(T,\phi) = (K_1 + K_2 \phi^m)(1 - \phi)^n \tag{3}$$

$$K_i = A_i \exp\left(-\frac{\Delta E_i}{RT^*}\right) \quad i = 1, 2 \tag{4}$$

 K_1 and K_2 are Arrhenius rate functions while m and n are dimensionless cure-fitting parameters. Equation 4 shows that the rate functions are dependent on activation energies ΔE_1 and ΔE_2 as well as the universal gas constant R and absolute

temperature T^* . Cure kinetics characterization techniques outlined in Shah et al. [3, 19] were employed with DSC to predict the degree of cure progression of the EPON 862/TETA system. These constants can be found in Table I.

TARIFI	CURF KINETICS	CONSTANTS FOR	RESIN SYSTEM EPON 862/TETA	

A_1	$\mathbf{A_2}$	$\Delta \mathrm{E}_1$	$\Delta \mathrm{E}_2$	m	n
(1/sec)	(1/sec)	(kJ/mol)	(kJ/mol)	(-)	(-)
242E+06	9.04E-02	72.5	11.5	0.92	1.75

Specimen Preparation for 3D-DIC Measurement

The specimen preparation for EPON 862/TETA for 3D-DIC experimentation is incredibly time-sensitive. First, the EPON 862 resin was degassed in a vacuum chamber for approximately 15 minutes. The TETA hardener was then integrated into the resin and stirred thoroughly to achieve a homogeneous mixture. The hardener reacts with the resin immediately upon contact. Therefore, a timer was started as soon as the mixing began to track the gelation. The EPON 862/TETA system was then degassed for an additional 15 minutes to remove any air bubbles produced by stirring. The specimen container was prepped with a fitted Teflon sheet to enforce a stress-free boundary condition during this process. The degassed mixture was then poured into the specimen container. A stochastic pattern (i.e., black speckle dots on a white background or vice versa) was then applied directly to the resin surface. Two case studies were conducted to observe chemical shrinkage:

- (1) Pre-Gelation Case: Strain measurement throughout the entire reaction. A black stochastic pattern was administered to the liquid resin surface with spray-paint.
- (2) Post-Gelation Case: Strain measurement only after gelation is reached. Upon gelation (approximately 40 minutes) the gelled resin surface was given a white spray-paint background before the stochastic pattern was implemented.

A schematic illustration of the prepared specimen is given in Figure 2.

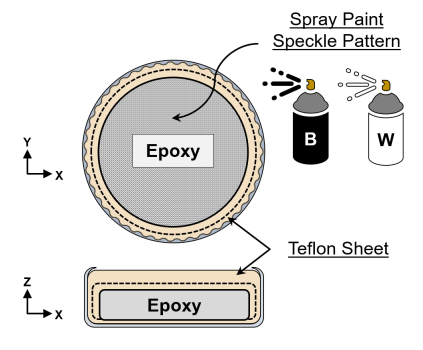


Figure 2. Graphic illustration of the prepared specimen.

3D-DIC Principles and Experimental Methods

Three-dimensional digital image correlation (3D-DIC) is a non-contacting, full-field, and photogrammetric measuring technique. It enables the extraction of surface strain, displacement, and geometry profiles from images obtained with a synchronized stereo camera pair system [45]. 3D-DIC tracks the displacement of a physical point P, with coordinates (X_P, Y_P, Z_P) in the global XYZ coordinate system, on the surface of a targeted object between a reference state and altered configuration as it is represented in the camera coordinate system (i.e., the retinal plane $x_i', y_i', 0$ in pixel units) [46]. The 3D space can then be obtained by combining the coordinates of point P in the two cameras' retinal planes with the intrinsic and extrinsic parameters using triangulation [47]. A schematic of the 3D-DIC setup is shown below in Figure 3.

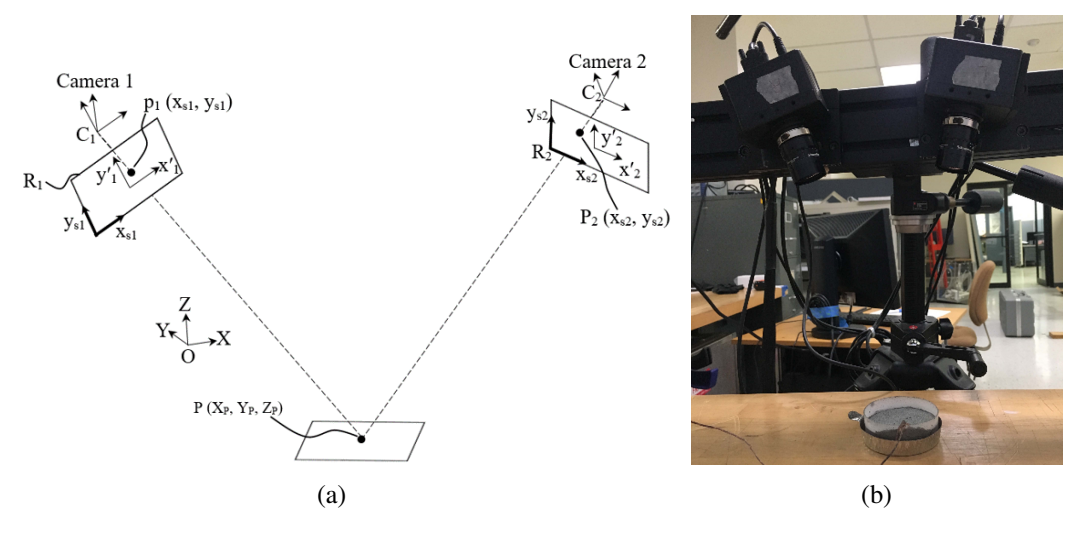


Figure 3. (a) Schematic illustration of 3D-DIC pinhole camera model transformations and (b) experimental setup with trial specimen.

Using the stochastic pattern outlined in the previous section, the relative position of each target is tracked as the surface deforms over time. For example, each image can be examined as a matrix of natural integers, where white pixels have a gray-scale level of 0 and black pixels have a gray-scale level of 100 [48]. A single value in a pattern is not necessarily unique, thus a square neighborhood of pixels, such as facets, is employed where each facet is a set of distinguishing correlation areas defined across the measuring region. As facets are typically 15-50 pixels squared, several dots of the stochastic pattern are included. The center of each facet is a measurement point that can be regarded as an extensometer. The position of these facets is tracked throughout each consecutively acquired image, and the 3D coordinates are then calculated for the entire area of interest.

For all surface elements, the deformation gradient tensor F was introduced to map the undeformed line elements dX into the deformed line elements dx:

$$d\mathbf{x} = \mathbf{F} \cdot d\mathbf{X} \tag{5}$$

The deformation gradient was then decomposed into the rotation matrix ${\bf R}$ and the right stretch tensor ${\bf U}$ such that:

$$\mathbf{F} = \mathbf{R} \cdot \mathbf{U} \tag{6}$$

Linear strain values were then recorded directly from the stretch tensor:

$$\varepsilon = \mathbf{U} - \mathbf{I} \tag{7}$$

The DIC system chosen for this study included two Megapixel FWX201 series digital cameras manufactured by Baumer GmBH using a 1/1.8" interline progressive charge coupled device (CCD) monochrome image sensors with a resolution of 1626×1236 pixels and a pixel size of $4.4 \times 4.4 \times 10^{-6}$ m [49]. The cameras were fitted with 12 mm focal length lenses manufactured by Schneider Optics, Inc. The 3D-DIC system was positioned to have a base distance of $12 \times 10 \times 10^{-2}$ m, a working distance of approximately $32.0 \times 10 \times 10^{-2}$ m, and a separation angle of about 27° . For all performed tests, image capture took place every 30 seconds during the first hour of measurement, and every 60 seconds for an additional two hours. This was done to ensure that more data could be collected during the initial phase of strain measurement for both pre-gelation and post-gelation cases. It should be noted that it was not possible to evaluate the noise floor of the measurement during testing due to the velocity of the chemical reaction taking place as the resin system was curing.

RESULTS AND DISCUSSION

Three tests were conducted for each case, yielding a total of six shrinkage tests. The ARAMIS acquisition software was used to collect full-field strain data that was then further processed in MATLAB. Figure 4 displays snapshots of the cure strain evolution captured with 3D-DIC.

Figure 4 indicates that some strain evolution exists prior to gelation that is not captured by post-gelation shrinkage tests. However, there were notable boundary effects that manifested from some of the resin slipping past the Teflon sheet during curing, thus adhering to the specimen container. This made it difficult to find an area of interest unaffected by the boundaries. Post-gelation strain fields captured by 3D-DIC have a homogeneous distribution with negligible boundary effects. Minor areas of missing optical data were also observed for this case. Linear cure strains ε_{xx} , ε_{yy} , and ε_{zz} were extracted from ARAMIS to plot strain component contour plots, as shown in Figure 5.

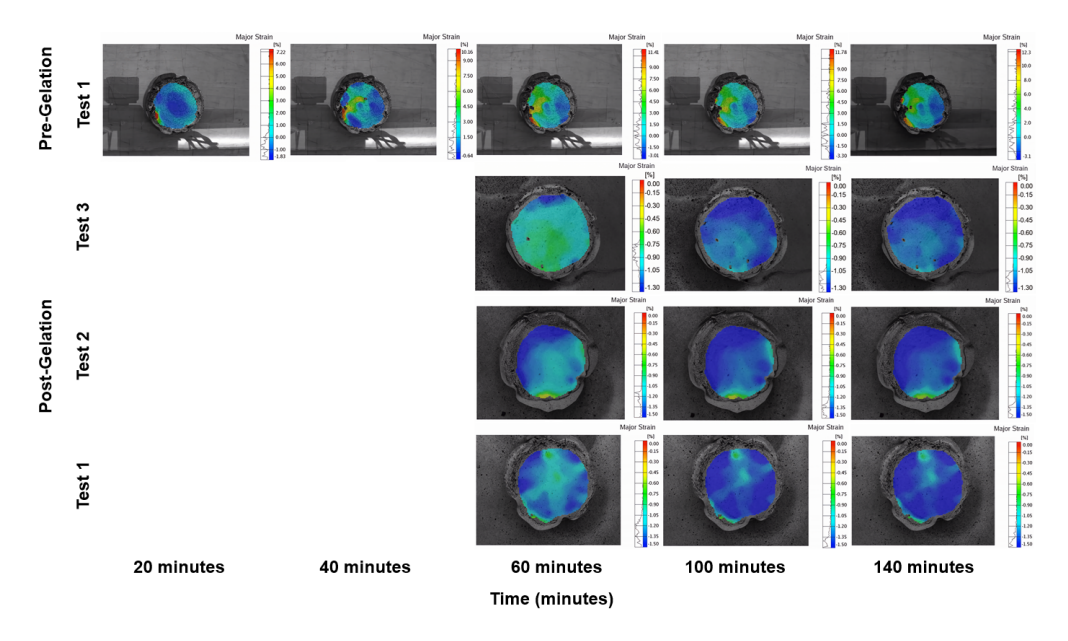


Figure 4. Visualization of cure strain development from 3D-DIC measurements for resin system EPON 862/TETA.

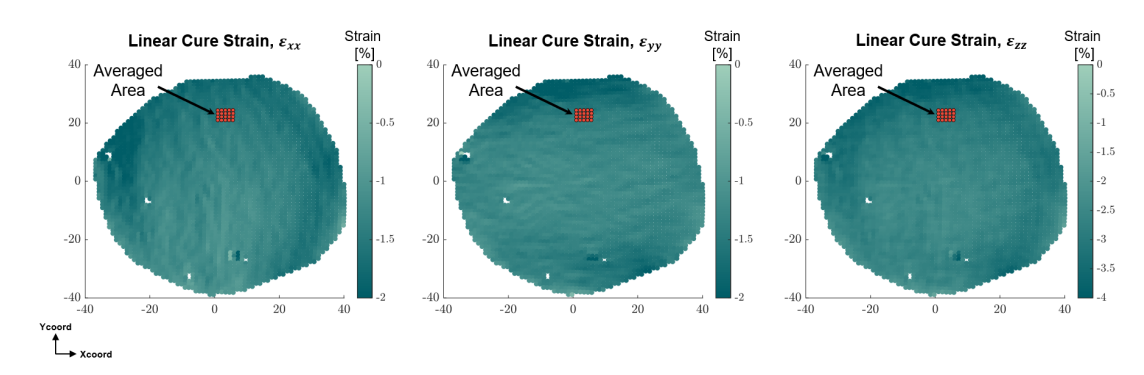


Figure 5. Post-gelation 3D-DIC linear cure strain contours post-processed with MATLAB.

It is evident from these contour plots that 3D-DIC is highly accurate in the in-plane (ε_{xx} and ε_{yy}) directions. The linear in-plane cure strains highly compare across all three post-gelation shrinkage tests. Approximately 20 data points were sampled from the in-plane strain contour plots (see Figure 5) to plot the linear shrinkage components ε_{xx} , ε_{yy} , and ε_{zz} . It can be seen from Figure 5 that the through-thickness cure strains are nearly twice as high as the in-plane strains. This is due to the fact that 3D-DIC experiments have a lower accuracy in the out-of-plane direction than in the in-plane. Degree of cure evolution was predicted using the cure kinetics parameters determined from DSC (see Table I). Gelation for these tests occurred between 35 and 50 minutes depending on ambient room temperatures. Figure 6 shows the linear shrinkage evolution from 3D-DIC experiments for the EPON 862/TETA system with respect to time and degree of cure.

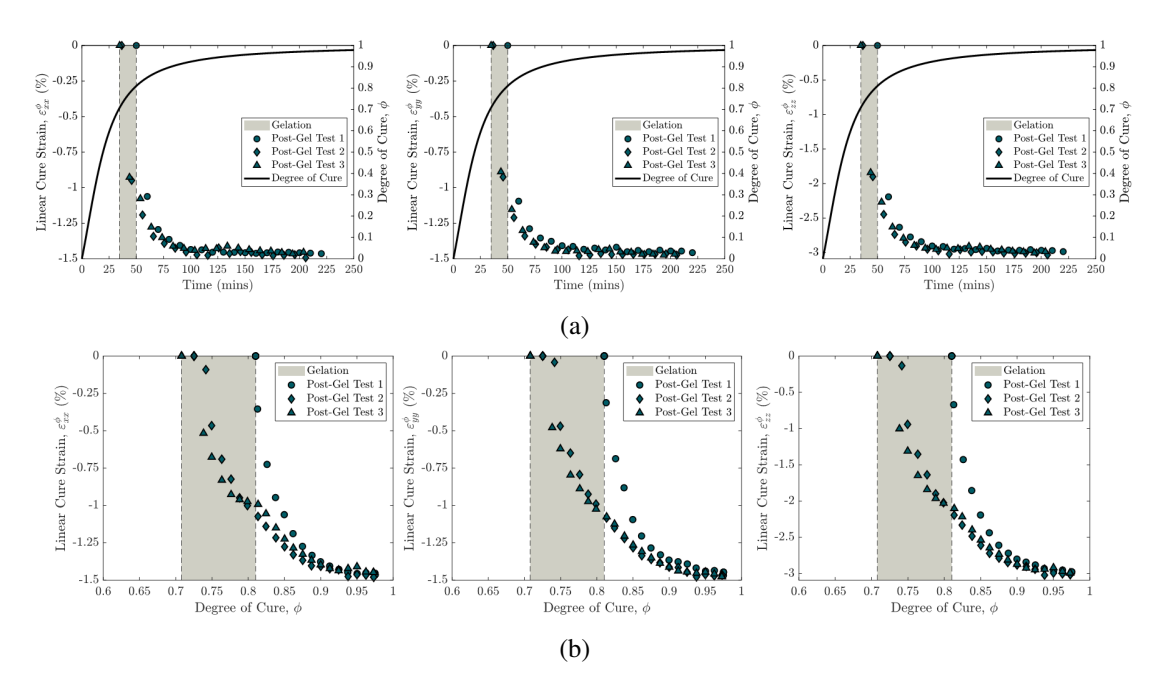


Figure 6. Post-gelation 3D-DIC linear shrinkage for EPON 862/TETA plotted against (a) time and (b) degree of cure.

Post-gelation experiments took between 200 and 220 minutes. In-plane 3D-DIC results yielded a final linear shrinkage of approximately -1.5% at degree of cure $\phi \approx$ 0.97. Figure 6(b) shows that the linear shrinkage evolves somewhat bilinearly with respect to degree of cure. 3D-DIC is highly capable of capturing in-plane strains to provide a more detailed relationship between chemical shrinkage and degree of cure.

Figure 7 shows the linear cure strain contour plots from 3D-DIC pre-gelation tests. Two of these tests exhibited paint cracking induced by the exothermic chemical reaction during curing.

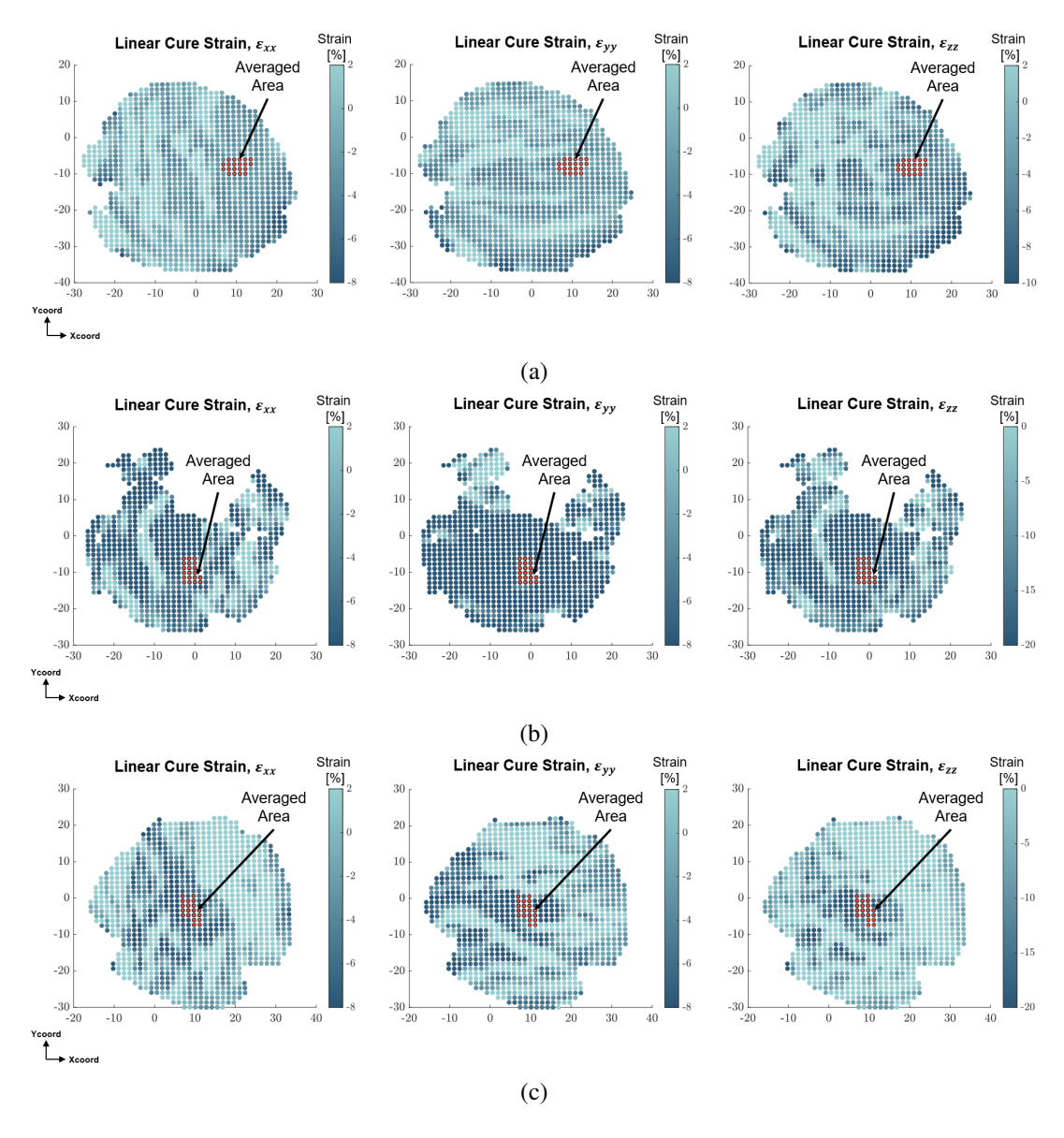


Figure 7. Pre-gelation 3D-DIC linear cure strain contours post-processed with MATLAB for (a) Test 1, (b) Test 2, and (c) Test 3.

Out-of-plane strains are once again higher than in-plane strains due to the decrease in through-thickness implicit in 3D-DIC measurement. This variability is more pronounced for the pre-gelation case because more of the chemical reaction was captured during curing, therefore creating more opportunity for variances to manifest due to boundary effects and paint cracking. One of the pre-gelation tests also experienced significant paint cracking upon gelation that resulted in some data loss in subsequent images, as seen in Figure 7(b). The presence of these boundary and surface imperfections indicate that the strain contours shown in Figure 7 are more indicative of the macroscopic behavior of the resin rather than the chemical shrinkage intrinsic to the material. However, it is still pertinent to observe this in-situ behavior of the resin, and even more so prior to gelation. For this reason, the in-situ linear cure strain evolution is shown below in Figure 8 and compared with post-gelation linear cure strains to observe notable trends. Note that post-gelation final strain values were

shifted to match those of their corresponding pre-gelation tests.

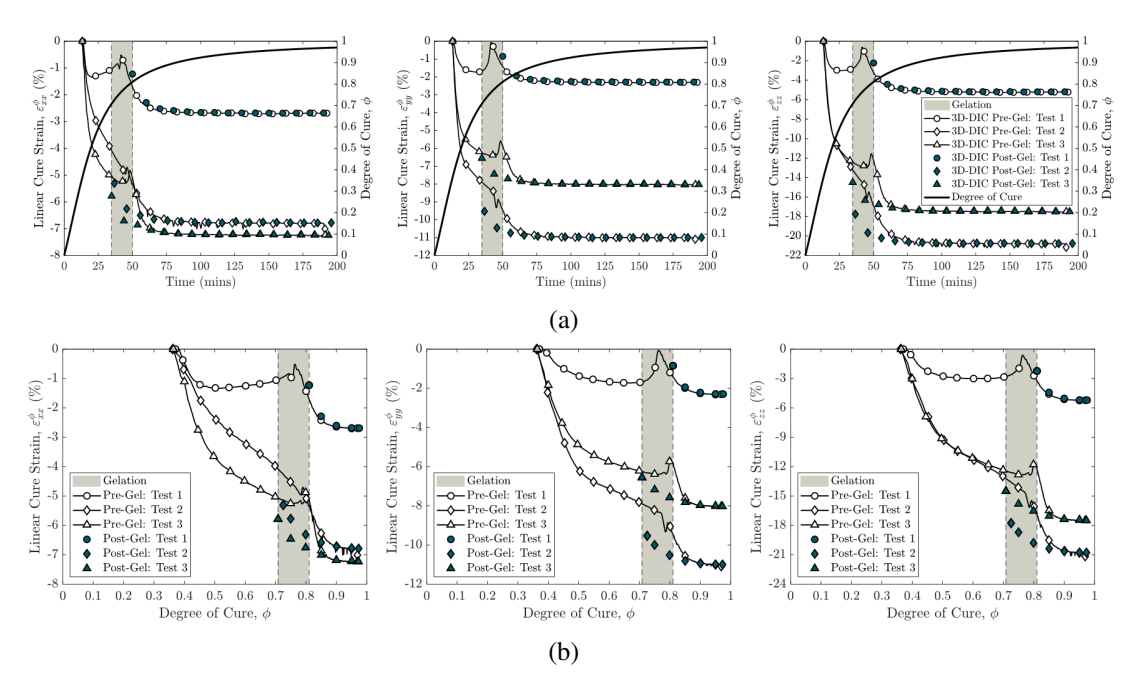


Figure 8. Pre- and post-gelation 3D-DIC linear cure strains for EPON 862/TETA plotted against (a) time and (b) degree of cure.

The pre-gelation linear cure strains exhibited in Figure 8 are clearly shown to be nonzero prior to gelation. One test reveals that the rate of strain evolution is negative at the start of 3D-DIC data acquisition, then becomes positive and approaches such that the strain zero at about 10 minutes prior to gelation. Local peaks occur close to gelation across all three pre-gelation tests, after which the linear cure strains evolves similarly to trends displayed by the post-gelation experiments. Two tests that experienced paint cracking during curing show a notable drop in linear cure strain at the start of the experiment. These pre-gelation 3D-DIC tests illustrate how the mechanical constraint imposed by the geometry or by the presence of reinforcements (such as carbon or glass fibers) plays a key role in quantifying in-situ strain behavior during curing. Moreover, these tests legitimize the application of 3D-DIC to monitor cure-induced in-situ dimensional changes.

CONCLUSIONS

This work proposed an innovative approach to measure chemical shrinkage with three-dimensional digital image correlation (3D-DIC) through the application of a spray-painted speckle pattern directly to the resin surface. Full-field strain was captured during curing for thermosetting resin system EPON 862/TETA under a post-gelation case and a pre-gelation case. Cure kinetics parameters were obtained with DSC to predict degree of cure. Post-gelation linear cure strain contours showed excellent in-plane agreement. The precision of out-of-plane 3D-DIC strain measurements was estimated to be a factor of two across the post- and pre-gelation

test cases. Pre-gelation linear strain contours showed a larger variance in-plane strains due to the mechanical constraints imposed on the resin during curing which emphasize the demand for computational methods to accurately predict cure-induced strain evolution in thermoset PMCs. In conclusion, 3D-DIC presents itself as a powerful optical solution to measure post-gelation volumetric shrinkage and observe pre-gelation in-situ strain behavior during curing, enabled by the novel implementation of a spray-painted stochastic pattern.

ACKNOWLEDGMENTS

The authors are grateful for the support of the National Science Foundation and Air Force Office of Scientific Research under grant number IIP-1826232.

REFERENCES

- 1. Beauson, J., B. Madsen, C. Toncelli, P. Brøndsted, and J. I. Bech. 2016, "Recycling of shredded composites from wind turbine blades in new thermoset polymer composites," *Composites Part A: Applied Science and Manufacturing*, 90:390–399.
- 2. Dorigato, A. 2021, "Recycling of thermosetting composites for wind blade application," *Advanced Industrial and Engineering Polymer Research*, 4(2):116–132.
- 3. Shah, S. P., S. U. Patil, C. J. Hansen, G. M. Odegard, and M. Maiarù. 2021, "Process modeling and characterization of thermoset composites for residual stress prediction," *Mechanics of Advanced Materials and Structures*, pp. 1–12.
- 4. Ramakrishna, S., J. Mayer, E. Wintermantel, and K. W. Leong. 2001, "Biomedical applications of polymer-composite materials: a review," *Composites science and technology*, 61(9):1189–1224.
- 5. Madhav, H., N. Singh, and G. Jaiswar. 2019, "Thermoset, bioactive, metal–polymer composites for medical applications," in *Materials for biomedical engineering*, Elsevier, pp. 105–143.
- 6. Iftekhar, A. 2004, "Biomedical composites," *Standard handbook of biomedical engineering and design*, pp. 1–17.
- 7. Biswal, T., S. K. BadJena, and D. Pradhan. 2020, "Synthesis of polymer composite materials and their biomedical applications," *Materials Today: Proceedings*, 30:305–315.
- 8. Badria, A., D. J. Hutchinson, N. Sanz del Olmo, and M. Malkoch. 2022, "Acrylate-free tough 3D printable thiol-ene thermosets and composites for biomedical applications," *Journal of Applied Polymer Science*, 139(43):e53046.
- 9. Hollaway, L. 2010, "A review of the present and future utilisation of FRP composites in the civil infrastructure with reference to their important in-service properties," *Construction and building materials*, 24(12):2419–2445.
- 10. Das, S. 2001, The cost of automotive polymer composites: a review and assessment of DOE's lightweight materials composites research, vol. 47, Oak Ridge National Laboratory Oak Ridge, TN, USA.
- 11. Palmer, J. 2009, "Mechanical recycling of automotive composites for use as reinforcement in thermoset," *PhD in Engineering dissertation, University of Exeter, UK.*
- 12. Friedrich, K. and A. A. Almajid. 2013, "Manufacturing aspects of advanced polymer

- composites for automotive applications," Applied Composite Materials, 20:107–128.
- 13. Soutis, C. 2005, "Fibre reinforced composites in aircraft construction," *Progress in aerospace sciences*, 41(2):143–151.
- 14. Katnam, K. B., L. Da Silva, and T. Young. 2013, "Bonded repair of composite aircraft structures: A review of scientific challenges and opportunities," *Progress in Aerospace Sciences*, 61:26–42.
- 15. D'Mello, R. J., A. M. Waas, M. Maiaru, and R. Koon. 2020, "Integrated computational modeling for efficient material and process design for composite aerospace structures," in *AIAA Scitech 2020 Forum*, p. 0655.
- Shah, S., S. Patil, P. Deshpande, A. Krieg, K. Kashmari, et al. 2020, "Multiscale modeling for virtual manufacturing of thermoset composites," in AIAA Scitech 2020 Forum, p. 0882.
- 17. Maiaru, M. 2018, "Effect of uncertainty in matrix fracture properties on the transverse strength of fiber reinforced polymer matrix composites," in 2018 AIAA/ASCE/AHS/ASC Structures, Structural Dynamics, and Materials Conference, p. 1901.
- 18. SHAH, S. and M. MAIARU. 2018, "Microscale analysis of virtually cured polymer matrix composites accounting for uncertainty in matrix properties during manufacturing," in *Proceedings of the American Society for Composites Thirty-third Technical Conference*.
- 19. Shah, S. P. and M. Maiarù. 2021, "Effect of manufacturing on the transverse response of polymer matrix composites," *Polymers*, 13(15):2491.
- 20. Deshpande, P., S. Shah, S. Patil, K. Kashmari, M. OLAYA, *et al.* 2020, "Multiscale Modelling of the cure process in thermoset polymers using ICME," in *Proceedings of the American Society for Composites â*€" *Thirty-fifth Technical Conference*.
- 21. PATIL, S., S. SHAH, P. DESHPANDE, K. KASHMARI, M. OLAYA, *et al.* 2020, "Multi-scale Approach to Predict Cure-Induced Residual Stresses in an Epoxy System," in *Proceedings of the American Society for Composites â€" Thirty-fifth Technical Conference*.
- 22. Patil, S. U., S. P. Shah, M. Olaya, P. P. Deshpande, M. Maiaru, *et al.* 2021, "Reactive molecular dynamics simulation of epoxy for the full cross-linking process," *ACS Applied Polymer Materials*, 3(11):5788–5797.
- 23. Gaikwad, P. S., A. S. Krieg, P. P. Deshpande, S. U. Patil, J. A. King, *et al.* 2021, "Understanding the Origin of the Low Cure Shrinkage of Polybenzoxazine Resin by Computational Simulation," *ACS Applied Polymer Materials*, 3(12):6407–6415.
- 24. Snow, A. W. and J. P. Armistead. 1994, "A simple dilatometer for thermoset cure shrinkage and thermal expansion measurements," *Journal of applied polymer science*, 52(3):401–411.
- 25. Li, C., K. Potter, M. R. Wisnom, and G. Stringer. 2004, "In-situ measurement of chemical shrinkage of MY750 epoxy resin by a novel gravimetric method," *Composites Science and Technology*, 64(1):55–64.
- Nawab, Y., N. Boyard, V. Sobotka, P. Casari, and F. Jacquemin. 2011, "A device to measure the shrinkage and heat transfers during the curing cycle of thermoset composites," in *Advanced Materials Research*, vol. 326, Trans Tech Publ, vol. 326, pp. 19–28.
- 27. Yu, H., S. Mhaisalkar, and E. Wong. 2005, "Cure shrinkage measurement of nonconductive adhesives by means of a thermomechanical analyzer," *Journal of electronic materials*, 34:1177–1182.
- 28. Bucknall, C. B., I. K. Partridge, and M. J. Phillips. 1991, "Mechanism of shrinkage control in polyester resins containing low-profile additives," *Polymer*, 32(4):636–640.

- 29. Hoa, S., P. Ouellette, and T. Ngo. 2009, "Determination of shrinkage and modulus development of thermosetting resins," *Journal of composite materials*, 43(7):783–803.
- 30. Ochi, M., K. Yamashita, and M. Shimbo. 1991, "The mechanism for occurrence of internal stress during curing epoxide resins," *Journal of Applied Polymer Science*, 43(11):2013–2019.
- 31. Magniez, K., A. Vijayan, and N. Finn. 2012, "Apparent volumetric shrinkage study of RTM6 resin during the curing process and its effect on the residual stresses in a composite," *Polymer Engineering & Science*, 52(2):346–351.
- 32. Giordano, M., A. Laudati, J. Nasser, L. Nicolais, A. Cusano, *et al.* 2004, "Monitoring by a single fiber Bragg grating of the process induced chemo-physical transformations of a model thermoset," *Sensors and Actuators A: Physical*, 113(2):166–173.
- 33. Karalekas, D., J. Cugnoni, and J. Botsis. 2008, "Monitoring of process induced strains in a single fibre composite using FBG sensor: A methodological study," *Composites part A: applied science and manufacturing*, 39(7):1118–1127.
- 34. Antonucci, V., M. Giordano, A. Cusano, J. Nasser, and L. Nicolais. 2006, "Real time monitoring of cure and gelification of a thermoset matrix," *Composites science and technology*, 66(16):3273–3280.
- 35. Haider, M., P. Hubert, and L. Lessard. 2007, "Cure shrinkage characterization and modeling of a polyester resin containing low profile additives," *Composites Part A: Applied Science and Manufacturing*, 38(3):994–1009.
- Nawab, Y., S. Shahid, N. Boyard, and F. Jacquemin. 2013, "Chemical shrinkage characterization techniques for thermoset resins and associated composites," *Journal of Materials Science*, 48:5387–5409.
- 37. Motagi, S., S. Chava, and S. Namilae. 2019, "In-situ Measurement of Resin Shrinkage in Epoxy Composite," *SAMPE 2019-Charlotte, NC, May 2019*.
- 38. Dupuis, A., J.-J. Pesce, J.-B. Marijon, S. Roux, and G. Régnier. 2022, "Use of a digital image correlation method for full-field shrinkage measurement in injection molding," *The Journal of Strain Analysis for Engineering Design*, 57(8):702–713.
- 39. Zündel, J., M. Sagerer, M. Frewein, and T. Krivec. 2021, "Characterization of prepreg shrinkage and investigation of its influence on warpage simulation," in 2021 22nd International Conference on Thermal, Mechanical and Multi-Physics Simulation and Experiments in Microelectronics and Microsystems (EuroSimE), IEEE, pp. 1–7.
- 40. Kravchenko, O. G., S. G. Kravchenko, A. Casares, and R. B. Pipes. 2015, "Digital image correlation measurement of resin chemical and thermal shrinkage after gelation," *Journal of Materials Science*, 50:5244–5252.
- 41. Motagi, S. and S. Namilae. 2021, "In-situ investigation of resin shrinkage in the composite manufacturing environment," *Applied Composite Materials*, 28:651–657.
- 42. Singer, G., G. Sinn, H. C. Lichtenegger, S. Veigel, M. Zecchini, *et al.* 2019, "Evaluation of in-situ shrinkage and expansion properties of polymer composite materials for adhesive anchor systems by a novel approach based on digital image correlation," *Polymer Testing*, 79:106035.
- 43. Bukenya, K., S. Shah, A. Sabato, and M. Maiaru. 2023, "Chemical Shrinkage Characterization during Curing through Three-Dimensional Digital Image Correlation,"
- 44. Kamal, M. and S. Sourour. 1973, "Kinetics and thermal characterization of thermoset cure," *Polymer Engineering & Science*, 13(1):59–64.
- 45. Sutton, M. A., J. J. Orteu, and H. Schreier. 2009, *Image correlation for shape, motion and deformation measurements: basic concepts, theory and applications*, Springer Science & Business Media.

- 46. Sutton, M. A., W. Wolters, W. Peters, W. Ranson, and S. McNeill. 1983, "Determination of displacements using an improved digital correlation method," *Image and vision computing*, 1(3):133–139.
- 47. Luo, P., Y. Chao, M. Sutton, and W.-H. Peters. 1993, "Accurate measurement of three-dimensional deformations in deformable and rigid bodies using computer vision," *Experimental mechanics*, 33:123–132.
- 48. Sabato, A., A. Sarrafi, Z. Mao, and C. Niezrecki. 2018, "Advancements in structural health monitoring using vision-based and optical techniques," in *Proc.*, 7th Asia-Pacific Workshop on Structural Health Monitoring.
- 49. Baumer, "FWX20C NeuroCheck Edition Digital Color Progressive Scan Camera," Accessed on March, 2019.